Title: Activity-dependent synapse elimination requires caspase-3 activation

Authors: Zhou Yu[1,2†*], Andrian Gutu[1†], Namsoo Kim[1], Erin K. O'Shea[1*]

Affiliations:

[1]Janelia Research Campus, Howard Hughes Medical Institute, Ashburn, VA, USA.

[2]Current address: Brigham and Women's Hospital, Harvard Medical School, Boston, MA, USA.

[†]These authors contributed equally.

[*]Correspondence: zyu3@bwh.harvard.edu, osheae@hhmi.org.

Abstract: During brain development, synapses are initially formed in excess and are later eliminated in an activity-dependent manner. Weak synapses are preferentially removed, but the mechanism linking neuronal activity to synapse removal is unclear. Here we show that, in the developing mouse visual pathway, inhibiting synaptic transmission induces postsynaptic activation of caspase-3. Caspase-3 deficiency results in defects in synapse elimination driven by both spontaneous and experience-dependent neural activity. Notably, caspase-3 deficiency blocks activity-dependent synapse elimination, as evidenced by reduced engulfment of inactive synapses by microglia. Furthermore, in a mouse model of Alzheimer's disease, caspase-3 deficiency protects against synapse loss induced by amyloid-β deposition. Our results reveal caspase-3 activation as a key step in activity-dependent synapse elimination during development and synapse loss in neurodegeneration.

Main Text:

Synapse elimination is the process in which excess synapses formed early during brain development are subsequently eliminated to form mature circuits (*1-3*). The outcome of synapse elimination depends on both spontaneous and experience-driven neural activity, with less active synapses being preferentially removed (*2, 4, 5*). However, the molecular mechanisms that connect neuronal activity to synapse elimination remain unclear. Previous studies have proposed that microglia and astrocytes, two major glial cell types of the brain, mediate activity-dependent synapse elimination by engulfing weak synapses (*6-14*), but it is unclear how glia can detect the "strength" of a synapse. A recent study proposed a molecular mechanism for activity-dependent synapse elimination in which the JAK2-STAT1 pathway is activated in inactive callosal projection neurons and regulates the removal of synapses and axons (*15*). However, the JAK-STAT pathway canonically functions through transcriptional regulation (*16*), which affects entire cells. If not all synapses made by a neuron are destined for removal (*3*), activation of the JAK2-STAT1 pathway alone may not provide sufficient elimination specificity. Therefore, other unidentified, locally-effective mechanisms likely exist that confer elimination specificity at the synapse level.

Caspase-3 is a protease crucial for the execution of apoptosis (*17*). In hippocampal neurons, transient activation of caspase-3 is required for long-term depression (LTD), a form of synaptic plasticity that induces long-lasting decreases in synaptic strength (*18*). Caspase-3 activation in apoptotic cells is also known to lead to the clearance of these cells by phagocytes (*19, 20*). These findings led us to hypothesize that caspase-3 may link synapse weakening with synapse removal by glia. Although caspases were

47 previously implicated in dendrite pruning in metamorphosis, degeneration-like axon
48 elimination, and the regulation of hippocampal spine density (*21-24*), the role of caspase-
49 3 in synapse elimination in response to neural activity was not clear. In this work, we
50 identify caspase-3 as a key molecule that is activated in postnatal development in
51 dendritic compartments upon synaptic weakening and is necessary for elimination of
52 weak synapses by microglia. Furthermore, we discovered that caspase-3 deficiency
53 protects against amyloid-β-induced synapse loss in a mouse model of Alzheimer's
54 disease, highlighting its significance not only in developmental synapse elimination but
55 also in adult neurodegenerative diseases.
56

57 **Tetanus toxin expression inactivates retinogeniculate synapses**

58 We chose the mouse retinogeniculate visual pathway as a model system to study
59 synapse elimination (*25*). In mice, retinal ganglion cells (RGCs) in each eye send out
60 axons to form retinogeniculate synapses with relay neurons in the dorsal lateral
61 geniculate nuclei (dLGN) of the thalamus on both sides of the brain (Fig. S1) (*25*). The
62 majority of RGC axons from each eye innervate the contralateral (on the side opposite to
63 the originating eye) dLGN while a smaller fraction innervate the ipsilateral (on the same
64 side as the originating eye) dLGN (Fig. S1) (*25*). Regions in each dLGN innervated by the
65 two eyes initially overlap but later segregate into eye-specific territories (Fig. S1). This
66 segregation process is a hallmark of retinogeniculate pathway development at the
67 morphological level and depends on synapse elimination and spontaneous RGC activity
68 (*25-27*).

69 To investigate the role of caspase-3 in activity-dependent synapse elimination, we
70 first needed to establish a method that could manipulate the strength of a subset of
71 retinogeniculate synapses. For this purpose, we used adeno-associated-virus (AAV) to
72 deliver a construct expressing tetanus toxin light chain (TeTxLC) under the control of the
73 neuron-specific human synapsin promoter (AAV-hSyn-TeTxLC) (Fig. 1A) (*28*). *In utero*
74 intraocular injection of AAV-hSyn-TeTxLC at embryonic day 15 (E15) leads to TeTxLC
75 expression in RGCs by the time of birth, blocking neurotransmitter release at
76 retinogeniculate synapses by cleaving synaptobrevin and leading to synapse inactivation
77 (*28, 29*). To label RGC axons and facilitate quantification, we co-injected AAVs that
78 express fluorescent proteins (mTurquiose2, eGFP, or tdTomato, depending on the
79 experiment) as anterograde tracers (Fig. 1A). These AAVs expressing fluorescent
80 proteins also served as controls for eye injections.

81 To validate the efficacy of our synapse inactivation method, we injected AAV-hSyn-
82 TeTxLC into the right eye of wildtype E15 embryos and analyzed the segregation of eye-
83 specific territories at postnatal day 8 (P8), when the segregation process is largely
84 complete (*25*). To quantify the overlap between eye-specific territories in an unbiased
85 manner, we applied a set of increasing thresholds to signals from both eyes (Fig. S2) (*30*).
86 For each threshold, we calculated a percentage overlap value as the ratio of the dLGN
87 area with signals from both eyes to the total dLGN area (Fig. S2 and Fig. S3). Consistent
88 with previous results (*26, 27*), inactivating right eye-associated retinogeniculate synapses
89 led to contraction of right eye-specific territories and expansion of left eye-specific
90 territories relative to control animals (Fig. S3A and S3B). Importantly, segregation of eye-
91 specific territories in TeTxLC-injected mice was significantly defective (Fig. S3C and S3D),

92 confirming that our method potently inactivated synapses and perturbed activity-
93 dependent refinement of the retinogeniculate pathway.
94
95 **Synapse inactivation induces postsynaptic caspase-3 activity**
96 Is caspase-3 activated in response to synapse weakening? To address this
97 question, we injected AAV-hSyn-TeTxLC into the right eyes of E15 embryos and looked
98 for caspase-3 activation in dLGNs of TeTxLC-injected mice at the age of P5 (a time when
99 synapse elimination is most active) (Fig. 1A) (*7, 25*). We used immunohistochemistry
100 against the cleaved and active form of caspase-3 to detect caspase-3 activity in the dLGN
101 area (*17*). If synapse inactivation leads to caspase-3 activation, we would expect higher
102 levels of caspase-3 activity in dLGNs with more inactivated synapses (Fig. 1A). In
103 agreement with this hypothesis, caspase-3 activity in left dLGNs of TeTxLC-injected
104 animals (dLGNs with the most inactivated synapses) was significantly higher compared
105 to that in right dLGNs of the same animals (dLGNs with intermediate amount of
106 inactivated synapses) (Fig. 1B, 1C, and 1E) and compared to that in dLGNs of animals
107 receiving control injections in the right eyes (dLGNs with no inactivation) (Fig. 1B, 1D,
108 and 1E). Reassuringly, caspase-3 activities in left and right dLGNs of control animals were
109 comparable (Fig. 1E), despite injections being administered only in the right eyes. This
110 suggests that surgical manipulation and viral transduction had no measurable contribution
111 to caspase-3 activation. These findings support the model that inactivation of
112 retinogeniculate synapses leads to caspase-3 activation.
113 Does inactivation of retinogeniculate synapses activate caspase-3 pre-synaptically
114 in RGCs or post-synaptically in dLGN relay neurons? Caspase-3 activity in dLGNs of

115 TeTxLC-injected mice was present either as discrete, punctate signals (Fig. 1F) or as
116 staining of entire cells (Fig. 1B and Fig. S4Bi-iii). Both types of signals were more
117 abundant in dLGNs with strong synapse inactivation than in control dLGNs (Fig. 1B, 1D
118 and 1F). Intriguingly, punctate caspase-3 activity was not found within TeTxLC-expressing
119 RGC axons (Fig. 1G). Instead, punctate caspase-3 activity closely juxtaposed inactivated
120 axon terminals (Fig. 1G) and co-localized with the dendritic marker MAP2 (Fig. S4A). In
121 the case where caspase-3 was activated in entire cells, the cells were positive for the
122 neuronal marker NeuN (Fig. S4C) and possessed relatively large round somas and
123 multipolar dendritic arbors (Fig. S4Bi-iii), all of which are characteristics of dLGN relay
124 neurons (*31, 32*). These observations suggest that caspase-3 activation triggered by
125 synapse inactivation occurs predominantly in the dendritic compartments of dLGN relay
126 neurons that are postsynaptic to the inactivated synapses.

127 Although morphologically distinct, localized and whole-cell caspase-3 activity may
128 be mechanistically linked. In support of this, we observed transitional states of caspase-
129 3 activation where multiple dendrites of a relay neuron were positive for active caspase-
130 3 without the cell body becoming apoptotic (an example is shown in Fig. S4Biv),
131 suggesting that whole-cell caspase-3 activation may arise from accumulation of local
132 caspase-3 activity. Such transitions might be particularly relevant in dLGNs that receive
133 the majority of TeTxLC-expressing axons, as systematic silencing of synapses could lead
134 to widespread caspase-3 activation in the postsynaptic neuron, potentially overwhelming
135 negative regulatory mechanisms that normally keep caspase-3 activation localized (*24,*
136 *33-35*). While our data cannot determine which form of caspase-3 activation plays a more
137 significant role in the normal development of the visual pathway, the infrequent

138 occurrence of whole-cell caspase-3 activation in control dLGNs (Figure 1D) -- which
139 undergo normal synapse elimination -- suggests that localized caspase-3 activation is
140 necessary to drive synapse elimination under physiological conditions.
141
142 **Caspase-3 activation at weak synapses requires the presence of strong synapses**
143 Previous experiments have manipulated RGC neuronal activities and
144 demonstrated that, regardless of the absolute level of RGC activity, the dLGN territory of
145 less active RGCs always contracted relative to that of more active RGCs (*26, 27*). This
146 observation suggests that the outcome of synapse elimination is driven by competitive
147 interactions between strong and weak synapses. Consistent with this idea, a recent study
148 demonstrated that elimination of weak synapses in callosal projections occurred only
149 when other strong synapses are present (*28, 36*).
150 To test if caspase-3 activation at weak synapses requires the presence of strong
151 synapses, we designed two experimental conditions. In the first condition, we inactivated
152 RGCs only in the right eye, leading to the presence of both active (from the left eye) and
153 inactive (from the right eye) synapses in the dLGN (Fig. 2A). We termed this condition
154 “single inactivation”. In the second condition, we inactivated RGCs in both eyes, leading
155 to the presence of only inactive synapses in the dLGN (Fig. 2A). We termed this condition
156 “dual inactivation”. We also included a control condition where no RGCs were inactivated
157 (Fig. 2A). We first confirmed that, in accordance with previous findings (*26, 37*),
158 segregation of eye-specific territories was disrupted in the dual inactivation condition (Fig.
159 S5A-D). We then measured dLGN caspase-3 activity in control, single, and dual
160 inactivation conditions. Intriguingly, while dLGN caspase-3 activity was significantly higher

161 in the single inactivation condition compared to that in the control (Fig. 2B and 2C), dLGN
162 caspase-3 activity in the dual inactivation condition was not significantly different from that
163 in the control (Fig. 2B and 2C) and was significantly lower than that in the single
164 inactivation condition (Fig. 2B and 2C). Although not reaching statistical significance,
165 dLGN caspase-3 activity on average was still higher in the dual inactivation condition
166 compared to the control (Fig. 2C), possibly due to incomplete inactivation of
167 retinogeniculate synapses, or interaction between weak retinogeniculate synapses and
168 strong synapses from other pathways, or additional mechanisms that activate caspase-3
169 independently of interactions between weak and strong synapses. These results suggest
170 that interaction between weak and strong synapses is required for caspase-3 activation
171 to occur at weak synapses.
172

173 **Caspase-3 is required for segregation of eye-specific territories**

174 Is synapse inactivation-induced caspase-3 activity important for synapse
175 elimination in the retinogeniculate pathway? To address this question, we investigated
176 whether segregation of eye-specific dLGN territories is defective if caspase-3 activation
177 does not occur. Since we were unable to find a Cre-expressing mouse line that
178 satisfactorily depletes caspase-3 in dLGN relay neurons, we used full-body caspase-3
179 deficient (*Casp3*$^{-/-}$) mice (*38, 39*). These mice were backcrossed to congenicity on the
180 C57Bl/6J background and were viable, fertile, and did not exhibit overt abnormalities (*39*).

181 To measure segregation of eye-specific territories, we injected the eyes of
182 *Casp3*$^{+/+}$ and *Casp3*$^{-/-}$ littermate mice at P9 with fluorophore-conjugated cholera toxin
183 subunit B (CTB), using a different fluorophore for each eye. CTB molecules bind to

184 ganglioside molecules on RGC surfaces and anterogradely label RGC axon terminals
185 (*40*). At P10, when CTB labeling and eye-specific segregation were complete (*25, 30*),
186 we collected the brains and imaged eye-specific territories in each dLGN. By visual
187 inspection, eye-specific territories in *Casp3*$^{+/+}$ dLGNs overlapped minimally (Fig. 3A). In
188 contrast, *Casp3*$^{-/-}$ dLGNs showed clear defects in the separation of eye-specific territories
189 (Fig. 3B) (*41*). We then quantified eye-specific segregation as described previously
190 (Figure S2) and found that percentage overlap in *Casp3*$^{-/-}$ dLGNs was consistently higher
191 than that in *Casp3*$^{+/+}$ dLGNs across all thresholds (Fig. 3C and D). Importantly, the fold
192 difference and statistical significance of the difference in percentage overlap between the
193 two groups of animals increased as the cutoff threshold increased (Fig. 3D), suggesting
194 the defects observed in *Casp3*$^{-/-}$ animals cannot be attributed to artifacts generated from
195 background noise.

196 As RGCs are known to undergo extensive apoptosis during the first week of
197 postnatal development (*42, 43*), we wondered if caspase-3 deficiency might block RGC
198 turnover and result in more RGC inputs in the dLGN, thereby confounding the overlap
199 analysis. To address this concern, we quantified the density of RGCs in whole-mount
200 retinae using a RGC marker, RBPMS (Fig. S6A) (*44*). Reassuringly, RGC densities in
201 retinae of *Casp3*$^{+/+}$ and *Casp3*$^{-/-}$ mice were not different (Fig. S6B), indicating that RGC
202 apoptosis still occurred at normal rates in the absence of caspase-3, presumably through
203 redundant mechanisms.

204 It is also possible that caspase-3 deficiency might confound the overlap analysis
205 by affecting the number of dLGN relay neurons. Therefore, we used NeuN staining to
206 visualized relay neurons in dLGNs of *Casp3*$^{+/+}$ and *Casp3*$^{-/-}$ mice and confirmed that relay

207 neuron density is not significantly altered by caspase-3 deficiency (Figure S7). Notably,
208 this observation indicates that, during normal development, synapse weakening does not
209 induce widespread whole-cell caspase-3 activation in dLGN relay neurons, corroborating
210 the idea that localized caspase-3 activity drives synapse elimination in dLGN. Collectively,
211 our findings suggest that caspase-3 is required for normal segregation of eye-specific
212 territories in dLGN.
213
214 **Caspase-3 is required for retinogeniculate circuit refinement**
215 Segregation of eye-specific territories in the mouse dLGN occurs prior to eye
216 opening (which happens at ~P13) and relies predominantly on spontaneous RGC activity
217 (*25*). After eye opening, sensory-dependent RGC activity drives a second phase of
218 refinement at the circuit level (*25*). At the time of eye opening, each dLGN relay neuron
219 receives numerous weak RGC inputs. With visual experience, a minority of these inputs
220 are strengthened while other weak inputs are eliminated, so that by P30 only a few
221 (typically ≤3) strong RGC inputs innervate each dLGN relay neuron (*25*).
222 To test if caspase-3 is required for visual experience-driven circuit refinement, we
223 prepared acute brain slices from P30 *Casp3*$^{+/+}$ and *Casp3*$^{-/-}$ littermate mice and
224 investigated the electrophysiological properties of retinogeniculate synapses (Fig. S8A)
225 (*45, 46*). We stimulated the optic tract while recording both AMPA receptor (AMPAR)- and
226 NMDA receptor (NMDAR)-mediated excitatory postsynaptic currents (EPSCs) in dLGN
227 relay neurons (Fig. S8A and Fig. 4A-B). By gradually increasing the stimulation intensity
228 on the optic tract, we recruit individual RGC axons in a serial manner (Fig. S8A).
229 Excitation of each RGC axon triggers a step increase in the EPSC amplitude (Fig. S8A),

230 allowing us to infer RGC input numbers by counting steps in EPSC response curves (Fig.
231 4C and S9A). In agreement with previous studies, retinogeniculate circuits in *Casp3*$^{+/+}$
232 animals were refined, with dLGN relay neurons most frequently receiving 2 strong RGC
233 inputs, and the great majority of neurons receiving no more than 3 inputs (Fig. 4A, 4C
234 and S9A). In contrast, RGC input counts of dLGN relay neurons in *Casp3*$^{-/-}$ animals
235 followed a long-tailed distribution that was significantly right-shifted from that of *Casp3*$^{+/+}$
236 animals (Fig. 4C and S9A). The majority of *Casp3*$^{-/-}$ relay neurons received more than 3
237 inputs (Fig. 4B-C and S9A), and many inputs elicited only small increments in EPSC
238 amplitude (Fig. 4B). Additionally, we examined maximum EPSC amplitude (Fig. S9B-C),
239 AMPAR-EPSC to NMDAR-EPSC ratio (Fig. S9D), and fiber fraction (Fig. S9E) (*46*) in
240 *Casp3*$^{+/+}$ and *Casp3*$^{-/-}$ mice. We found no significant difference between the two groups
241 of animals, suggesting that the defective circuit refinement in *Casp3*$^{-/-}$ animals was not
242 due to the lack of retinogeniculate synapse maturation but instead an inability to eliminate
243 weak synapses.

244 An increased number of RGC inputs innervating dLGN relay neurons in *Casp3*$^{-/-}$
245 mice should correspond to greater numbers of presynaptic release sites and should result
246 in more frequent spontaneous release of neurotransmitters. To test this prediction, we
247 measured miniature EPSCs (mEPSCs) in dLGN relay neurons of *Casp3*$^{+/+}$ and *Casp3*$^{-/-}$
248 mice (Fig. 4D). We found that mEPSCs in *Casp3*$^{-/-}$ neurons occurred more frequently (Fig.
249 4E), with a greater fraction of them having small amplitudes (Fig. 4F). These results mirror
250 previous measurements in hippocampal CA1 neurons in Casp3$^{-/-}$ mice (*24*). Overall, our
251 observations are consistent with the model where caspase-3 deficiency impairs the
252 removal of weak synapses, leading to greater number of inputs on dLGN relay neurons.

253 As an additional way to probe retinogeniculate circuit refinement, we measured
254 paired-pulse response ratios (PPRs) in dLGN relay neurons (Fig. S8B and Fig. 4G-H) (*45,*
255 *47*). The retinogeniculate circuit typically generates PPRs that are smaller than one due
256 to depletion of neurotransmitters (Fig. S8B) (*45, 47*). If there is an increase in the number
257 of release sites in *Casp3*$^{-/-}$ mice, we expect more available neurotransmitters and larger
258 PPRs (Fig. S8C) (*47*). Indeed, we observed higher PPRs in *Casp3*$^{-/-}$ dLGN relay neurons
259 (Fig. 4D-E), suggesting that defective synapse elimination resulted in more RGC release
260 sites in *Casp3*$^{-/-}$ mice. Taken together, our results demonstrate that caspase-3 is required
261 for experience-driven retinogeniculate circuit refinement.
262

263 **Caspase-3 deficiency impairs synapse elimination by microglia**

264 Our results demonstrate that proper synapse elimination in the retinogeniculate
265 pathway requires caspase-3 activity. Previous studies have shown that microglia and
266 astrocytes engulf weak synapses during the process of synapse elimination (*7, 10*). We
267 therefore sought to determine whether caspase-3 activation is required for synapse
268 elimination by microglia and/or astrocytes.

269 If synapse elimination by microglia depends on caspase-3 activation, then
270 microglia in *Casp3*$^{-/-}$ mice should engulf less synaptic material. Similar to a previous study
271 (*7*), we utilized the *Cx3cr1-Gfp* transgenic mouse line to visualize microglia *in vivo.* In this
272 line, the native *Cx3cr1* promoter drives *Gfp* expression and specifically labels microglia
273 in the brain (Fig. 5A) (*48*). We labeled RGC axon terminals by injecting fluorophore-
274 conjugated CTB in the eyes of P4 *Casp3*$^{+/-}$; *Cx3cr1-Gfp*$^{+/-}$ and *Casp3*$^{-/-}$; *Cx3cr1-Gfp*$^{+/-}$
275 littermate pups (*Casp3*$^{+/-}$ instead of *Casp3*$^{+/+}$ mice were used to enable more efficient

276 breeding) (*7*). At P5, the brains were harvested and the dLGN imaged (Figure 5A).
277 Microglia in *Casp3*$^{-/-}$; *Cx3cr1-Gfp*$^{+/-}$ mice had small soma and thin processes, indicating
278 that caspase-3 deficiency did not result in microglial activation (Fig. 5B). This is further
279 validated by immunohistochemical analysis of microglia in caspase-3 deficient mice (Fig.
280 S10A-D). To quantify synapse engulfment, we isolated volumes corresponding to
281 microglia and RGC axon terminals in the dLGN (Fig. 5B) and calculated the volume of
282 RGC terminals that were fully enclosed in each microglia (Fig. 5C). As expected, we
283 observed that microglia in *Casp3*$^{-/-}$; *Cx3cr1-Gfp*$^{+/-}$ mice engulfed significantly less axonal
284 material compared to those of *Casp3*$^{+/-}$; *Cx3cr1-Gfp*$^{+/-}$ littermates (Fig. 5B-C). The same
285 trend was observed when RGC axon terminals originating from the two eyes were
286 analyzed separately (Fig. S11A-B). As the engulfment capacity of microglia is limited by
287 their size, we normalized the volume of engulfed synaptic material in each microglia to
288 the microglial volume (Fig. 5D). Microglia in both groups of mice are comparable in size
289 (Fig. S11C), and the defective synaptic engulfment in *Casp3*$^{-/-}$ mice persisted after
290 normalization to microglial volume (Fig. 5D). Additionally, the same defect was observed
291 when engulfment values were averaged and reported by animal (Fig. S11D). Taken
292 together, our results demonstrate that microglia-mediated synapse elimination depends
293 on caspase-3.

294 To test whether caspase-3 activation is also required for astrocyte-mediated
295 synapse elimination, we used the *Aldh1l1-Gfp* transgenic mouse line, where *Gfp*
296 expression specifically labels astrocytes (Fig. S12A) (*49*). We again labeled RGC axon
297 terminals in *Casp3*$^{+/-}$; *Aldh1l1-Gfp*$^{+/-}$ and *Casp3*$^{-/-}$; *Aldh1l1-Gfp*$^{+/-}$ littermate mice with CTB
298 conjugates (Fig. S12A). Astrocytes were present in the P5 dLGN at a much higher density

299 than microglia and possess very fine processes (Fig. S12A). To ensure segmentation
300 fidelity, we only analyzed astrocyte cell bodies and their proximal processes (Fig. S12B).
301 Unexpectedly, we found that the volume of axonal material engulfed by astrocytes was
302 comparable in the two groups of mice (Fig. S12C). The same trend was observed when
303 we normalized the volume of engulfed synaptic material to astrocyte volume (Fig. S12D-
304 E). It is possible that, by using *Casp3*$^{+/-}$ mice instead of *Casp3*$^{+/+}$ mice as controls, we
305 have obscured some defects in astrocyte-mediated synapse elimination. Nevertheless,
306 given that astrocyte-mediated synapse elimination did not show clear dependence on
307 caspase-3, we focused on measuring synapse engulfment by microglia as a readout of
308 preferential elimination of weak synapses.
309

310 **Removal of weak synapses by microglia requires caspase-3 activity**

311 If caspase-3 activation at weak synapses is important for synapse removal, then
312 in caspase-3 deficient mice, microglia should lose the ability to engulf weak synapses. To
313 test this hypothesis, we inactivated retinogeniculate synapses originating from right eyes
314 in *Casp3*$^{+/+}$ and *Casp3*$^{-/-}$ mice with AAV-hSyn-TeTxLC injections (Fig. 6A). A group of
315 animals was included for each genotype that received control injections. To measure
316 synapse engulfment by microglia, we labeled RGC axon terminals with CTB conjugates
317 and visualized microglia by immunostaining against Iba1, a marker specific for microglia
318 in the brain (Fig. 6B-G). According to our model, in TeTxLC-injected *Casp3*$^{+/+}$ mice,
319 microglia should preferentially engulf inactive retinogeniculate synapses originating from
320 the right eye (Fig. 6A), whereas in TeTxLC-injected *Casp3*$^{-/-}$ mice, synapses from the right
321 and the left eye should be engulfed at similar levels regardless of their strength (Fig. 6A).

322 To quantitatively detect engulfment of weak synapses by microglia, we compared
323 TeTxLC-injected and control-injected animals of the same genotype (Fig. 6B, C, and F).
324 We first calculated the ratio between the volume of right eye-originated RGC axon
325 terminals and left eye-originated terminals that were engulfed by each microglia. Then,
326 by comparing this right-to-left engulfment ratio in TeTxLC-injected vs. control-injected
327 animals, engulfment of inactive synapses could be detected as higher engulfment ratios
328 in TeTxLC-injected animals (Fig. 6F). It is worth noting confounding factors, such as
329 surgical manipulations, cancel out when calculating engulfment ratios, allowing
330 information pertaining only to substrate preference to be isolated.
331 Consistent with previous studies (*7*), in *Casp3*$^{+/+}$ mice inactivation of
332 retinogeniculate synapses from the right eye led to enhanced microglia-mediated
333 engulfment of right eye-originated RGC axon terminals but not left eye-originated
334 terminals (Fig. S13A-B), resulting in a significant increase in right-to-left engulfment ratios
335 in microglia of TeTxLC-injected animals compared to control-injected animals (Fig. 6B, C,
336 and F). In contrast, engulfment ratios were similar between TeTxLC-injected and control-
337 injected *Casp3*$^{-/-}$ mice (Fig. 6D, E and G and Fig. S13C-D), suggesting that microglia
338 could no longer distinguish between strong and weak synapses in the absence of
339 caspase-3 activation. These observations remain valid when data were averaged and
340 reported by animal (Fig. S13E-F). Summing the evidence obtained thus far, we propose
341 the activity-dependent caspase-3 activation is a crucial signaling event that integrates
342 upstream information about synaptic activity, takes place at weak/inactive synapses, and
343 leads to activity-dependent elimination of weak synapses by microglia.
344

345 **Caspase-3 deficiency protects against amyloid-β-induced synapse loss**

346 Lastly, we wanted to test if caspase-3 regulates synapse loss in neurodegenerative
347 diseases through mechanisms analogous to its role in activity-dependent synapse
348 elimination. To this end, we focused on Alzheimer's disease (AD). AD is the most common
349 cause of dementia (*50*), and synapse loss is the strongest correlate of cognitive decline
350 in AD patients (*51*). Accumulation and deposition of oligomeric or fibril amyloid-
351 β (Aβ) peptide has been proposed to be the cause of neurodegeneration in AD (*50*).
352 Intriguingly, oligomeric Aβ impairs long-term potentiation (LTP) (*52*), and this suppression
353 of LTP requires caspase-3 activation (*53*). Additionally, caspase-3 activation has been
354 linked to early synaptic dysfunction in an AD mouse model (*54*).

355 To test if synapse loss in AD is regulated by caspase-3, we utilized the APP/PS1
356 mouse line, in which amyloid precursor protein (APP) and presenilin 1 (PS1) carrying
357 mutations associated with early-onset familial AD are overexpressed in CNS neurons (*55*).
358 We observed that female *App/Ps1*$^{+/-}$ mice developed amyloid deposits in the
359 hippocampus and cortex by 5 months (Fig. S14Aii), and that the amyloid burden
360 worsened by 6 months (Fig. S14Aiii). In male *App/Ps1*$^{+/-}$ mice, amyloid deposits only
361 became apparent at 6 months and occurred at a lower level compared to age-matched
362 females (Fig. S14Aiv-v). We focused on analyzing *App/Ps1*$^{+/-}$ female mice in subsequent
363 experiments to obtain robust phenotypes. To quantify synapse loss, we labeled
364 presynaptic and postsynaptic compartments in the dentate gyrus of 6 month-old *App/Ps1*$^{-}$
365 $^{/-}$ and *App/Ps1*$^{+/-}$ littermates by detecting synaptic vesicle protein 2 (SV2) and Homer1,
366 respectively, and selected multiple fields of interest per animal for imaging analysis while
367 avoiding regions adjacent to amyloid deposits (Fig. S15). We fitted ellipsoids to SV2 and

368 Homer1 signals to identify pre- and post-synaptic puncta and defined synapses as
369 Homer1-SV2 puncta pairs that were less than 300 nm apart (Fig. 7A). We observed that
370 synapse density in *App/Ps1*$^{+/-}$ mice was significantly reduced compared to that in
371 *App/Ps1*$^{-/-}$ littermate controls (Fig. 7A-B), and that this reduction could be attributed to
372 lower densities of both pre- and post-synaptic puncta in *App/Ps1*$^{+/-}$ mice (Fig. S16A-B).
373 We then crossed APP/PS1 mice to caspase-3 deficient mice and quantified synapse
374 density in 6 month-old *Casp3*$^{-/-}$; *App/Ps1*$^{-/-}$ and *Casp3*$^{-/-}$; *App/Ps1*$^{+/-}$ littermate mice (Fig.
375 S15). We observed that, in the caspase-3 deficient background, overexpression of mutant
376 APP and PS1 no longer resulted in a reduction in the density of synapses (Fig. 7C-D) or
377 pre-/post-synaptic puncta (Fig. S16C-D), suggesting that caspase-3 activity is required
378 for Aβ-induced synapse loss in the APP/PS1 mouse model. Intriguingly, levels of amyloid
379 deposition were comparable between *App/Ps1*$^{+/-}$ and *Casp3*$^{-/-}$; *App/Ps1*$^{+/-}$ mice (Fig.
380 S14Avi and B), and reactive microglia were observed near amyloid deposits regardless
381 of caspase-3 deficiency (Fig. S17), indicating that protection conferred by caspase-3
382 deficiency against Aβ-induced synapse loss might not require inhibition of amyloid
383 accumulation or microgliosis. We also investigated whether Aβ accumulation induced
384 elevated levels of caspase-3 activity. We analyzed 4, 5, and 6 month-old *App/Ps1*$^{-/-}$ and
385 *App/Ps1*$^{+/-}$ mice but only observed robust upregulation of caspase-3 activity in the dentate
386 gyrus of a subset of 4 month-old *App/Ps1*$^{+/-}$ mice (Fig. S18A-C). Upregulated caspase-3
387 activity in these mice remained in a punctate pattern without inducing neuronal death (Fig.
388 S18D-F). It is possible that Aβ transiently induces caspase-3 activation in *App/Ps1*$^{+/-}$ mice,
389 but stochasticity in the onset and duration of such induction prevents reliable detection
390 with our sample size and temporal resolution. Overall, our results demonstrate caspase-

391 3 as an important regulator of Aβ-induced synapse loss and a potential therapeutic target
392 for AD treatment.
393

394 ## Discussion:

395 **A model for caspase-3 dependent synapse elimination**

396 Our findings support a model where competitive interaction between strong
397 synapses and weak synapses in the retinogeniculate pathway triggers caspase-3
398 activation in the postsynaptic compartments of weak synapses. Caspase-3 activation
399 results in the removal of weaker synaptic connections by microglia, thereby facilitating the
400 establishment of mature circuits in the visual pathway.
401

402 **Mechanisms of activity-dependent caspase-3 activation**

403 In the experiment where we demonstrated activity-dependent caspase-3 activation,
404 we inactivated all retinogeniculate synapses from one eye to induce sufficiently high
405 caspase-3 activity that can be discerned from background. Widespread caspase-3 activity
406 induced by such strong inactivation at multiple sites in a given cell likely self-amplifies
407 through positive feedback (*35*) and overwhelms negative regulation mechanisms (e.g.,
408 ubiquitin-dependent proteasomal degradation (*24, 33, 34*)), leading to the observed
409 apoptosis of entire dLGN relay neurons (Fig. 1B). However, apoptotic neurons were
410 infrequently observed in the dLGN of control animals (Fig. 1D and 2B), and caspase-3
411 deficiency does not significantly alter dLGN relay neuron numbers (Fig. S7), suggesting
412 that during normal development, activity-dependent caspase-3 activation is
413 predominantly localized and generally does not lead to neuronal death.

414 Intriguingly, synaptic inactivation in our experiment was achieved through TeTxLC
415 expression in presynaptic RGCs, but caspase-3 activation was observed in postsynaptic
416 relay neurons. Conversely, while caspase-3 is activated in the postsynaptic compartment,
417 we were able to detect defects in synapse elimination using assays that measure
418 presynaptic inputs. These observations suggest that activity-dependent caspase-3
419 activation requires synaptic transmission, and that caspase-3 dependent synapse
420 elimination is not strictly axonal or dendritic but involves both pre- and post-synaptic
421 compartments. An important limitation of this study is that experiments in full-body *Casp3*$^{-}$
422 $^{/-}$ mice cannot query the roles of caspase-3 in presynaptic and postsynaptic compartments
423 separately. Future experiments that perturb caspase-3 activation and other signaling
424 events specifically in the pre- or post-synaptic compartments are needed to reveal more
425 detailed mechanisms of activity-dependent synapse elimination.
426 The observation that activity-dependent caspase-3 activation requires the
427 presence of both weak and strong synapses resonates with previous research
428 demonstrating that relative synaptic efficacy biases the outcome of synapse elimination
429 during development of neuromuscular junctions and the callosal pathway (*15, 36, 56, 57*).
430 However, the mechanisms linking synaptic competition with caspase-3 activation remains
431 elusive. During LTD, caspase-3 is activated through mitochondrial release of cytochrome-
432 c (*18*). Whether synaptic competition could induce caspase-3 activation via mechanisms
433 such as calcium signaling, which regulates both neurotransmission and cytochrome-c
434 release (*58*), is an outstanding question.
435
436 **Link between caspase-3 activation and synapse engulfment by microglia**

437 How does caspase-3 activation at weak synapses lead to synapse engulfment by
438 microglia? Caspase-3 activation is known to trigger the display of apoptosis markers that
439 can be recognized by phagocytes (*19*). One of the best understood markers is
440 phosphatidylserine (PtdSer), a phospholipid that translocates from the cytoplasmic leaflet
441 of the plasma membrane to the exoplasmic leaflet during apoptosis (*19*). Importantly,
442 caspase-3 directly regulates the enzymes that translocate PtdSer through enzymatic
443 cleavage (*59, 60*). Two recent studies demonstrated that PtdSer is displayed on
444 retinogeniculate synapses during postnatal development, and microglia use the exposed
445 PtdSer as a cue to target and engulf synapses (*8, 9*). Whether PtdSer exposure is
446 upregulated in response to synapse weakening and whether caspase-3 activity is
447 required for such exposure are important questions that require further investigation.

448 The complement protein C1q has been observed to bind to PtdSer on apoptotic
449 cells and facilitate phagocytic clearance (*19*). Additionally, a previous study found
450 caspase-3 activity in C1q-positive synaptosomes (*61*), suggesting that C1q may bridge
451 caspase-3 activation and synapse elimination. However, we investigated C1q expression
452 and localization in the dLGN of P5 TeTxLC-injected mice but did not observe upregulation
453 of C1q abundance or colocalization between C1q and caspase-3 activity (data not shown).

454 It is often assumed in the literature that microglia directly engulf intact synapses,
455 but existing data also support an alternative model where microglia indirectly contribute
456 to synapse elimination by engulfing synaptic debris that is shed through neuron-
457 autonomous mechanisms (*62*). The observation that synaptic activity promotes microglial
458 engulfment through caspase-3 activation raises the possibility that weakened synapses
459 partially disintegrate through apoptosis-like mechanisms prior to being engulfed by

460 microglia. Further studies are needed to elucidate the intermediate steps between
461 caspase-3 activation and microglial engulfment of synapses.
462
463 **Caspase-3 as a potential target for AD treatment**
464 Our findings suggest that caspase-3 deficiency confers protection against Aβ-
465 induced synapse loss in a mouse model of AD. Notably, the absence of caspase-3 does
466 not seem to affect Aβ deposition or microglia reactivity, indicating that caspase-3 depletion
467 may mitigate synapse loss by directly countering Aβ-induced synaptic toxicity. Given the
468 prominence of Aβ and inflammation as targets for AD drug development (*63*), inhibiting
469 caspase-3 activity offers a potential alternative therapeutic strategy that could
470 complement and enhance current treatment approaches. Therefore, it is important to test
471 whether pharmacological inhibition of caspase-3 can effectively slow synapse loss and
472 cognitive decline in both mouse models of AD and human patients.
473
474 **Acknowledgement:** We thank Crystall Lopez, Benjamin Gantz, and Brooke Groff for help
475 with animal husbandry and breeding. We thank Sarah Lindo, Colin Morrow, Claire Boyer,
476 and Rae Demars for help with surgery. We thank Monique Copeland, Amy Hu, Morgan
477 Clarke, and Benjamin Foster for help with histology. We are also grateful to Sarah
478 Kivimaki and the Viral Tools team of Janelia Core Services for help with AAV preparation.
479 We thank Dr. Cagla Eroglu, Dr. Richard Axel, and Dr. David Clapham for comments on
480 the manuscript. This work is supported by the Howard Hughes Medical Institute.
481
482 **References:**

483 1. M. Kano, K. Hashimoto, Synapse elimination in the central nervous system. *Curr Opin*
484 *Neurobiol* **19**, 154-161 (2009).
485 2. T. E. Faust, G. Gunner, D. P. Schafer, Mechanisms governing activity-dependent synaptic
486 pruning in the developing mammalian CNS. *Nat Rev Neurosci* **22**, 657-673 (2021).
487 3. M. M. Riccomagno, A. L. Kolodkin, Sculpting neural circuits by axon and dendrite pruning.
488 *Annu Rev Cell Dev Biol* **31**, 779-805 (2015).
489 4. L. C. Katz, C. J. Shatz, Synaptic activity and the construction of cortical circuits. *Science* **274**,
490 1133-1138 (1996).
491 5. J. Y. Hua, S. J. Smith, Neural activity and the dynamics of central nervous system
492 development. *Nat Neurosci* **7**, 327-332 (2004).
493 6. B. Stevens *et al.*, The classical complement cascade mediates CNS synapse elimination.
494 *Cell* **131**, 1164-1178 (2007).
495 7. D. P. Schafer *et al.*, Microglia sculpt postnatal neural circuits in an activity and
496 complement-dependent manner. *Neuron* **74**, 691-705 (2012).
497 8. T. Li *et al.*, A splicing isoform of GPR56 mediates microglial synaptic refinement via
498 phosphatidylserine binding. *Embo J* **39**, e104136 (2020).
499 9. N. Scott-Hewitt *et al.*, Local externalization of phosphatidylserine mediates developmental
500 synaptic pruning by microglia. *Embo J* **39**, e105380 (2020).
501 10. W. S. Chung *et al.*, Astrocytes mediate synapse elimination through MEGF10 and MERTK
502 pathways. *Nature* **504**, 394-400 (2013).
503 11. D. K. Wilton, L. Dissing-Olesen, B. Stevens, Neuron-Glia Signaling in Synapse Elimination.
504 *Annu Rev Neurosci* **42**, 107-127 (2019).
505 12. W. S. Chung, N. J. Allen, C. Eroglu, Astrocytes Control Synapse Formation, Function, and
506 Elimination. *Cold Spring Harb Perspect Biol* **7**, a020370 (2015).
507 13. Q. Li, B. A. Barres, Microglia and macrophages in brain homeostasis and disease. *Nat Rev*
508 *Immunol* **18**, 225-242 (2018).
509 14. R. C. Paolicelli *et al.*, Synaptic pruning by microglia is necessary for normal brain
510 development. *Science* **333**, 1456-1458 (2011).
511 15. M. Yasuda, S. Nagappan-Chettiar, E. M. Johnson-Venkatesh, H. Umemori, An activity-
512 dependent determinant of synapse elimination in the mammalian brain. *Neuron* **109**,
513 1333-1349 e1336 (2021).
514 16. R. L. Philips *et al.*, The JAK-STAT pathway at 30: Much learned, much more to do. *Cell* **185**,
515 3857-3876 (2022).
516 17. D. R. McIlwain, T. Berger, T. W. Mak, Caspase functions in cell death and disease. *Cold*
517 *Spring Harb Perspect Biol* **5**, a008656 (2013).
518 18. Z. Li *et al.*, Caspase-3 Activation via Mitochondria Is Required for Long-Term Depression
519 and AMPA Receptor Internalization. *Cell* **141**, 859-871 (2010).
520 19. S. Y. Park, I. S. Kim, Engulfment signals and the phagocytic machinery for apoptotic cell
521 clearance. *Exp Mol Med* **49**, (2017).
522 20. L. A. Trouw, A. M. Blom, P. Gasque, Role of complement and complement regulators in the
523 removal of apoptotic cells. *Mol Immunol* **45**, 1199-1207 (2008).
524 21. D. W. Williams, S. Kondo, A. Krzyzanowska, Y. Hiromi, J. W. Truman, Local caspase activity
525 directs engulfment of dendrites during pruning. *Nat Neurosci* **9**, 1234-1236 (2006).

526 22. C. T. Kuo, S. Zhu, S. Younger, L. Y. Jan, Y. N. Jan, Identification of E2/E3 ubiquitinating
527 enzymes and caspase activity regulating Drosophila sensory neuron dendrite pruning.
528 *Neuron* **51**, 283-290 (2006).
529 23. D. J. Simon *et al.*, A caspase cascade regulating developmental axon degeneration. *J*
530 *Neurosci* **32**, 17540-17553 (2012).
531 24. A. Erturk, Y. Wang, M. Sheng, Local pruning of dendrites and spines by caspase-3-
532 dependent and proteasome-limited mechanisms. *J Neurosci* **34**, 1672-1688 (2014).
533 25. L. Liang, C. Chen, Organization, Function, and Development of the Mouse
534 Retinogeniculate Synapse. *Annu Rev Vis Sci* **6**, 261-285 (2020).
535 26. A. A. Penn, P. A. Riquelme, M. B. Feller, C. J. Shatz, Competition in retinogeniculate
536 patterning driven by spontaneous activity. *Science* **279**, 2108-2112 (1998).
537 27. D. Stellwagen, C. J. Shatz, An instructive role for retinal waves in the development of
538 retinogeniculate connectivity. *Neuron* **33**, 357-367 (2002).
539 28. M. Yasuda, S. Nagappan-Chettiar, H. Umemori, In utero intraocular AAV injection for early
540 gene expression in the developing rodent retina. *STAR Protoc* **2**, 100742 (2021).
541 29. G. Schiavo *et al.*, Tetanus and botulinum-B neurotoxins block neurotransmitter release by
542 proteolytic cleavage of synaptobrevin. *Nature* **359**, 832-835 (1992).
543 30. C. L. Torborg, M. B. Feller, Unbiased analysis of bulk axonal segregation patterns. *J Neurosci*
544 *Meth* **135**, 17-26 (2004).
545 31. T. E. Krahe, R. N. El-Danaf, E. K. Dilger, S. C. Henderson, W. Guido, Morphologically distinct
546 classes of relay cells exhibit regional preferences in the dorsal lateral geniculate nucleus
547 of the mouse. *J Neurosci* **31**, 17437-17448 (2011).
548 32. J. G. Parnavelas, E. J. Mounty, R. Bradford, A. R. Lieberman, The postnatal development of
549 neurons in the dorsal lateral geniculate nucleus of the rat: a Golgi study. *J Comp Neurol*
550 **171**, 481-499 (1977).
551 33. Y. E. Choi *et al.*, The E3 ubiquitin ligase cIAP1 binds and ubiquitinates caspase-3 and -7 via
552 unique mechanisms at distinct steps in their processing. *J Biol Chem* **284**, 12772-12782
553 (2009).
554 34. Y. Suzuki, Y. Nakabayashi, R. Takahashi, Ubiquitin-protein ligase activity of X-linked
555 inhibitor of apoptosis protein promotes proteasomal degradation of caspase-3 and
556 enhances its anti-apoptotic effect in Fas-induced cell death. *Proc Natl Acad Sci U S A* **98**,
557 8662-8667 (2001).
558 35. S. McComb *et al.*, Efficient apoptosis requires feedback amplification of upstream
559 apoptotic signals by effector caspase-3 or -7. *Sci Adv* **5**, eaau9433 (2019).
560 36. S. Nagappan-Chettiar, M. Yasuda, E. M. Johnson-Venkatesh, H. Umemori, The molecular
561 signals that regulate activity-dependent synapse refinement in the brain. *Curr Opin*
562 *Neurobiol* **79**, 102692 (2023).
563 37. F. M. Rossi *et al.*, Requirement of the nicotinic acetylcholine receptor beta 2 subunit for
564 the anatomical and functional development of the visual system. *Proc Natl Acad Sci U S A*
565 **98**, 6453-6458 (2001).
566 38. K. Kuida *et al.*, Decreased apoptosis in the brain and premature lethality in CPP32-
567 deficient mice. *Nature* **384**, 368-372 (1996).
568 39. C. Houde *et al.*, Caspase-7 expanded function and intrinsic expression level underlies
569 strain-specific brain phenotype of caspase-3-null mice. *J Neurosci* **24**, 9977-9984 (2004).

570 40. L. De Haan, T. R. Hirst, Cholera toxin: a paradigm for multi-functional engagement of
571 cellular mechanisms (Review). *Mol Membr Biol* **21**, 77-92 (2004).
572 41. N. Otsu, A Threshold Selection Method from Gray-Level Histograms. *IEEE Transactions on*
573 *Systems, Man, and Cybernetics* **9**, 62-66 (1979).
574 42. R. W. Young, Cell death during differentiation of the retina in the mouse. *J Comp Neurol*
575 **229**, 362-373 (1984).
576 43. B. Dreher, R. A. Potts, M. R. Bennett, Evidence that the early postnatal reduction in the
577 number of rat retinal ganglion cells is due to a wave of ganglion cell death. *Neurosci Lett*
578 **36**, 255-260 (1983).
579 44. A. R. Rodriguez, L. P. de Sevilla Muller, N. C. Brecha, The RNA binding protein RBPMS is a
580 selective marker of ganglion cells in the mammalian retina. *J Comp Neurol* **522**, 1411-1443
581 (2014).
582 45. C. Chen, W. G. Regehr, Developmental remodeling of the retinogeniculate synapse.
583 *Neuron* **28**, 955-966 (2000).
584 46. B. M. Hooks, C. Chen, Distinct roles for spontaneous and visual activity in remodeling of
585 the retinogeniculate synapse. *Neuron* **52**, 281-291 (2006).
586 47. W. G. Regehr, Short-term presynaptic plasticity. *Cold Spring Harb Perspect Biol* **4**, a005702
587 (2012).
588 48. S. Jung *et al.*, Analysis of fractalkine receptor CX(3)CR1 function by targeted deletion and
589 green fluorescent protein reporter gene insertion. *Mol Cell Biol* **20**, 4106-4114 (2000).
590 49. S. Gong *et al.*, A gene expression atlas of the central nervous system based on bacterial
591 artificial chromosomes. *Nature* **425**, 917-925 (2003).
592 50. D. S. Knopman *et al.*, Alzheimer disease. *Nat Rev Dis Primers* **7**, 33 (2021).
593 51. S. Meftah, J. Gan, Alzheimer's disease as a synaptopathy: Evidence for dysfunction of
594 synapses during disease progression. *Front Synaptic Neurosci* **15**, 1129036 (2023).
595 52. G. M. Shankar *et al.*, Amyloid-beta protein dimers isolated directly from Alzheimer's brains
596 impair synaptic plasticity and memory. *Nat Med* **14**, 837-842 (2008).
597 53. J. Jo *et al.*, Abeta(1-42) inhibition of LTP is mediated by a signaling pathway involving
598 caspase-3, Akt1 and GSK-3beta. *Nat Neurosci* **14**, 545-547 (2011).
599 54. M. D'Amelio *et al.*, Caspase-3 triggers early synaptic dysfunction in a mouse model of
600 Alzheimer's disease. *Nat Neurosci* **14**, 69-76 (2011).
601 55. J. L. Jankowsky *et al.*, Mutant presenilins specifically elevate the levels of the 42 residue
602 beta-amyloid peptide in vivo: evidence for augmentation of a 42-specific gamma secretase.
603 *Hum Mol Genet* **13**, 159-170 (2004).
604 56. M. Buffelli *et al.*, Genetic evidence that relative synaptic efficacy biases the outcome of
605 synaptic competition. *Nature* **424**, 430-434 (2003).
606 57. Y. I. Lee, Developmental neuromuscular synapse elimination: Activity-dependence and
607 potential downstream effector mechanisms. *Neurosci Lett* **718**, 134724 (2020).
608 58. C. Garrido *et al.*, Mechanisms of cytochrome c release from mitochondria. *Cell Death*
609 *Differ* **13**, 1423-1433 (2006).
610 59. J. Suzuki, D. P. Denning, E. Imanishi, H. R. Horvitz, S. Nagata, Xk-Related Protein 8 and CED-
611 8 Promote Phosphatidylserine Exposure in Apoptotic Cells. *Science* **341**, 403-406 (2013).
612 60. K. Segawa *et al.*, Caspase-mediated cleavage of phospholipid flippase for apoptotic
613 phosphatidylserine exposure. *Science* **344**, 1164-1168 (2014).

61. B. A. Gyorffy *et al.*, Local apoptotic-like mechanisms underlie complement-mediated synaptic pruning. *Proc Natl Acad Sci U S A* **115**, 6303-6308 (2018).
62. U. Eyo, A. V. Molofsky, Defining microglial-synapse interactions. *Science* **381**, 1155-1156 (2023).
63. P. van Bokhoven *et al.*, The Alzheimer's disease drug development landscape. *Alzheimers Res Ther* **13**, 186 (2021).

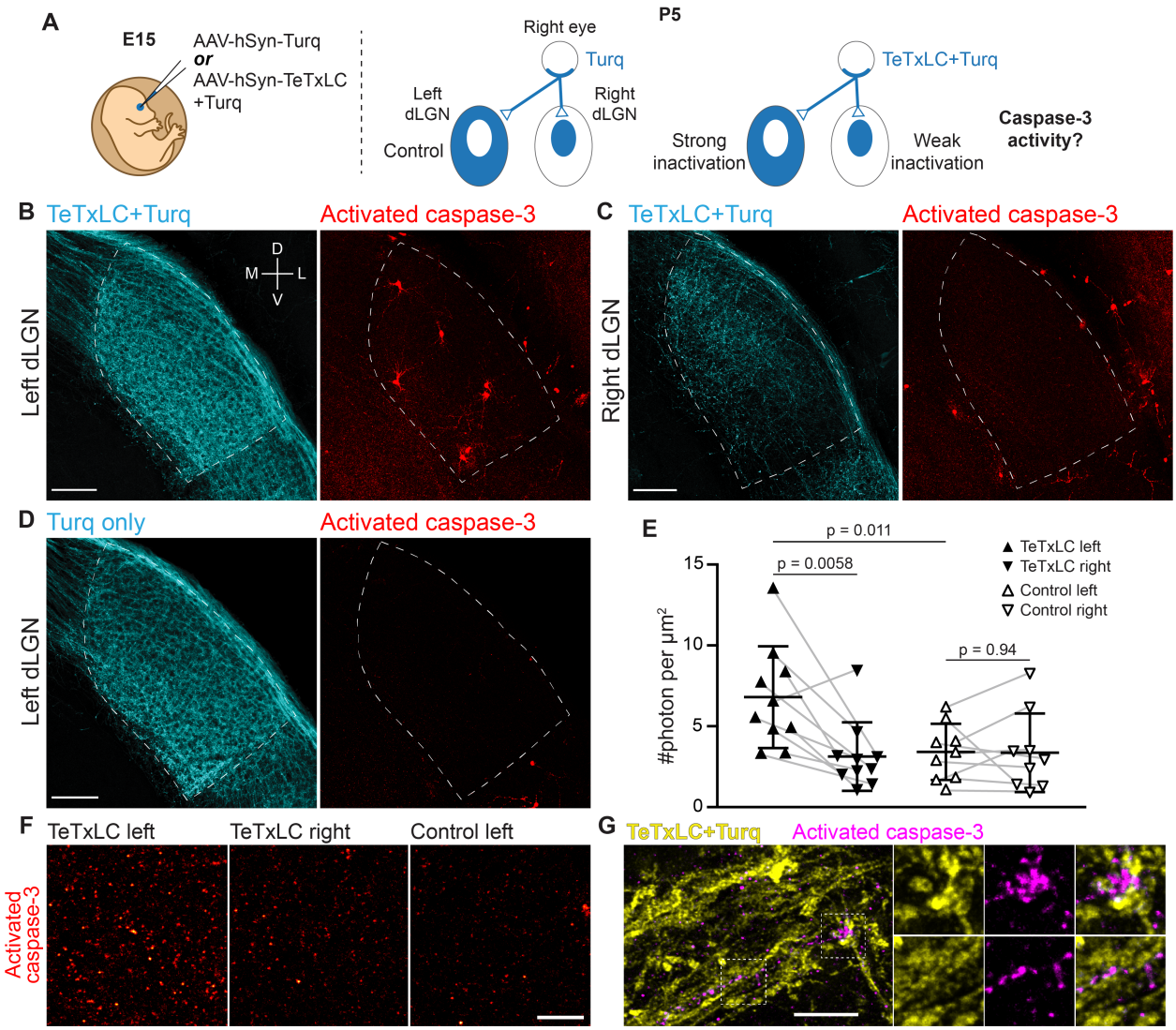

Figure 1. Inactivation of retinogeniculate synapses induces caspase-3 activity. (**A**) Schematics of experimental setup. AAVs expressing tetanus toxin light chain (TeTxLC) and/or mTurquiose2 (Turq) were injected into the right eye of E15 mice (left). By P5, retinogeniculate synapses in dLGN were inactivated to varying extents depending on injection and side (right). (**B**-**D**) Confocal images of Turq (left panels) and activated caspase-3 (right panels) in left dLGN (**B**) and right dLGN (**C**) of a TeTxLC-injected P5 animal and in left dLGN of a control P5 animal (**D**). Dotted lines delineate dLGN boundaries. Only signals within dLGNs were analyzed. Images from the same fluorescent channel were adjusted to the same contrast. The compass in **B** marks tissue orientation. Scale-bars: 100 µm. D, dorsal; V, ventral; M, medial; L, lateral. (**E**) Quantification of caspase-3 activity in indicated dLGNs. Activated caspase-3 signals in each dLGN (highlighted areas in **B**-**D**) were summed and normalized to dLGN area. Each point represents the result from one dLGN. Data from two dLGNs of the same animal were paired for analysis (grey lines). n=10 for TeTxLC-injected animals and n=9 for control animals. Mean and standard deviation (S.D.) are shown. P-values were calculated from two-tailed t-tests (paired when applicable). (**F**) Example images showing punctate caspase-3 activities in ventral-medial regions of indicated dLGNs. Images were adjusted to the same contrast. Scale-bar: 20 µm. (**G**) High-resolution images of dLGN showing TeTxLC-expressing RGC axons (yellow) and activated caspase-3 (magenta). Two regions of interest (dotted squares) are magnified to illustrate that caspase-3 activity was found juxtaposing TeTxLC-expressing axon terminals but not within them. Scale-bar: 5 µm.

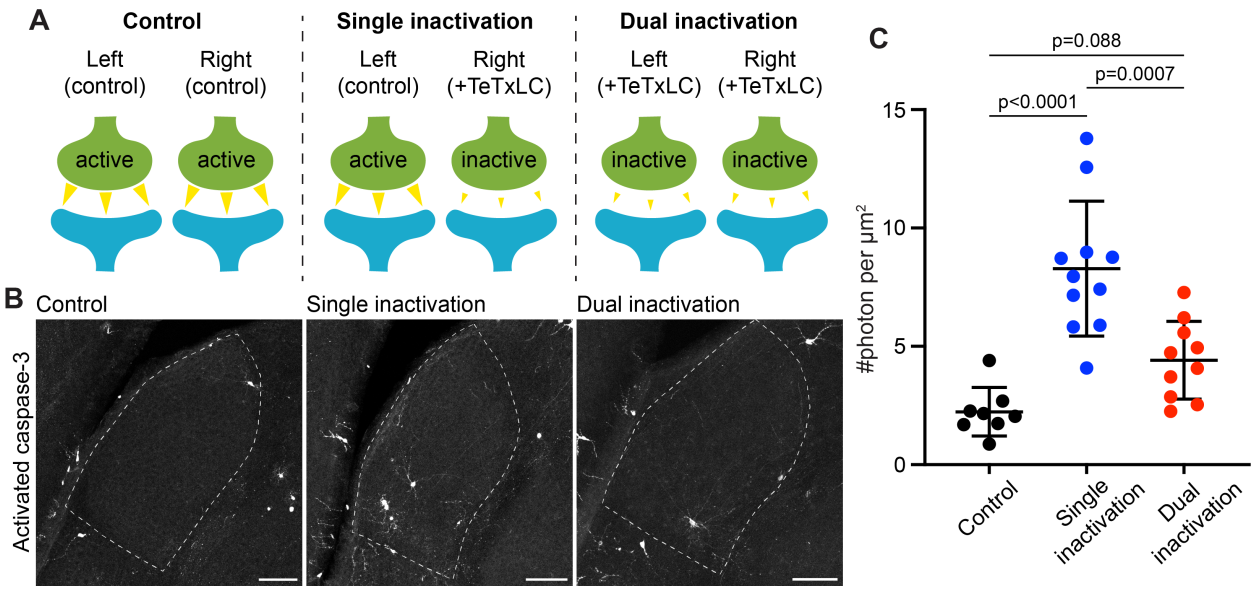

Figure 2. Caspase-3 activation at weak synapses requires the presence of strong synapses. (**A**) Schematics illustrating experimental conditions. No synapses are inactivated in the control (left); only synapses from right eyes are inactivated in single inactivation condition (middle); synapses from both right and left eyes are inactivated in dual inactivation condition (right). (**B**) Confocal images of P5 left side dLGNs in the three conditions showing caspase-3 activity in the dLGN. Dotted lines mark dLGN boundaries. Scale-bars: 100 µm. (**C**) Quantification of dLGN caspase-3 activity in the indicated conditions. Caspase-3 activity in each dLGN were summed and normalized to the dLGN area. For the single inactivation condition, values were from left dLGNs only. For the other two conditions, values from both dLGNs were averaged. n=8 animals for control, n=11 animals for single inactivation, and n=10 animals for dual inactivation. Mean and S.D. are shown. P-values were calculated from Tukey's multiple comparison tests.

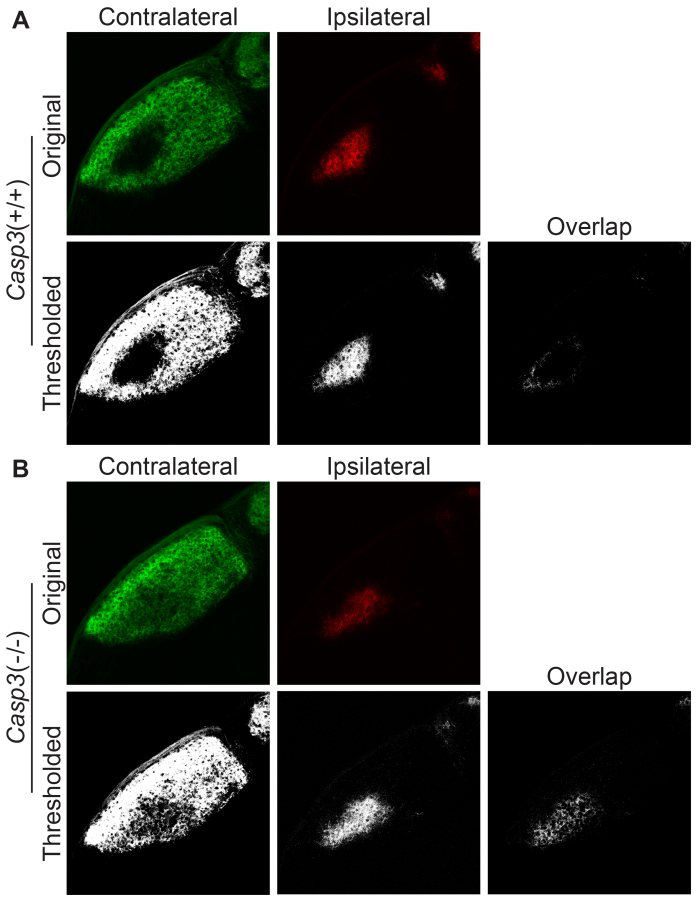

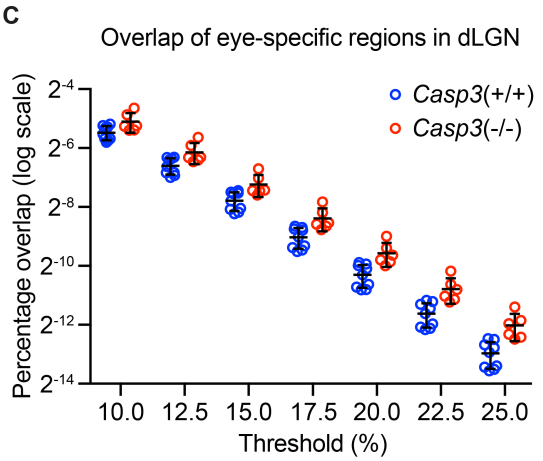

D

Threshold (%)	*Casp3*(+/+) mean	*Casp3*(-/-) mean	p-value
10.0	0.0224	0.0290	0.027
12.5	0.0103	0.0141	0.016
15.0	0.00453	0.00662	0.0095
17.5	0.00192	0.00298	0.0056
20.0	0.00079	0.00131	0.0034
22.5	0.00032	0.00057	0.0021
25.0	0.00012	0.00024	0.0015

Figure 3. Caspase-3 is required for segregation of eye-specific territories. (**A**-**B**) Representative confocal images of retinogeniculate inputs in the dLGN of P10 wild-type (**A**) and *Casp3*$^{-/-}$ (**B**) mice. Contralateral inputs are labeled with AlexaFlour488 (AF488) conjugated cholera toxin subunit B (CTB) and ipsilateral inputs with AF594-CTB. Original images were thresholded into 0-or-1 images using the Otsu method (*34*), and the overlap between thresholded contralateral and ipsilateral inputs is shown. (**C**) Percentage overlap between eye-specific territories in wildtype and *Casp3*$^{-/-}$ mice under a series of increasing signal cutoff thresholds. Note that the percentage overlap is plotted on a log scale. Each circle represents one animal. Mean and S.D. are shown. n=9 for wildtype mice and n=6 for *Casp3*$^{-/-}$ mice. (**D**) Mean percentage overlap values in wildtype and *Casp3*$^{-/-}$ mice and p-values of two-tailed t-tests between the two genotypes are listed for each cutoff threshold.

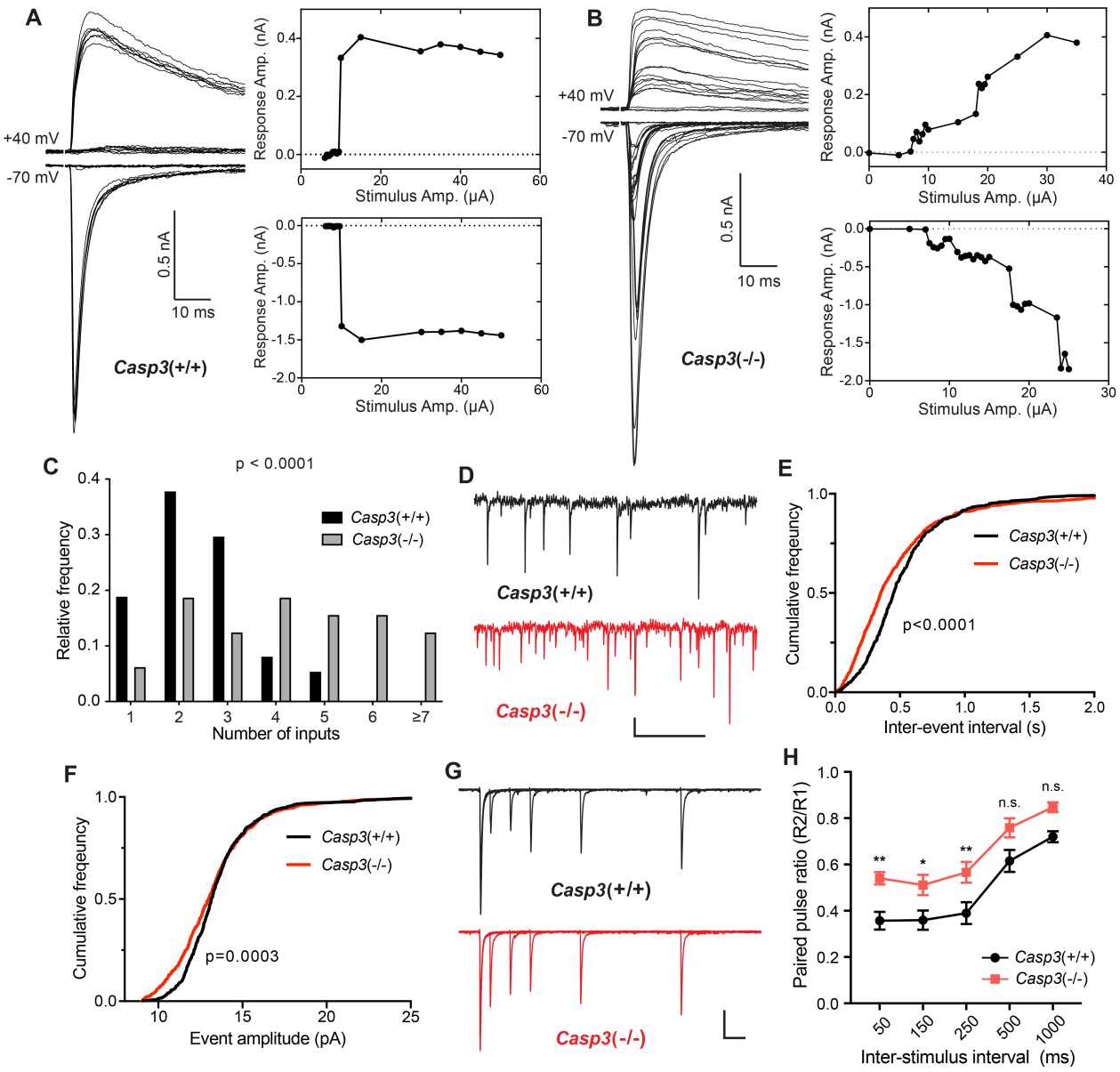

Figure 4. Caspase 3 is required for retinogeniculate circuit refinement. (**A**-**B**) Example recordings of dLGN relay neuron responses in P30 wildtype (**A**) and *Casp3*$^{-/-}$ (**B**) mice. Excitatory postsynaptic currents (EPSCs) were evoked by increasing stimulation currents in the optic tract. Both AMPAR-mediated inward current at -70 mV membrane potential and AMPAR and NMDAR-mediated outward current at +40 mV membrane potential are shown. Peak response amplitudes at each stimulation intensity are plotted to the right of recording traces. Scale bars represent 0.5 nA and 10 ms. (**C**) Distribution of RGC input numbers on individual dLGN relay neurons in wildtype and *Casp3*$^{-/-}$ mice. The number of RGC inputs was inferred by manually counting the number of steps in AMPAR-mediated EPSC response curves (lower right in **A** and **B**) while blind to the genotypes. P-value was calculated from two-tailed t-test. n=37 cells from 22 wildtype mice and n=32 cells from 16 *Casp3*$^{-/-}$ mice. (**D**) Example recordings of mEPSC measurements from wildtype and *Casp3*$^{-/-}$ mice. Scale-bars represent 0.5 s (horizontal) and 5 pA (vertical). (**E**-**F**) Cumulative distribution curves of inter-mEPSC intervals (**E**) and mEPSC amplitudes (**F**) in wildtype and *Casp3*$^{-/-}$ mice. P-values were calculated from Kolmogorov-Smirnov tests. n=16 cells from 4 wildtype mice and n=17 cells from 4 *Casp3*$^{-/-}$ mice. (**G**) Example recordings from paired pulse measurements at -70 mV membrane potential in wildtype and *Casp3*$^{-/-}$ mice. Traces from experiments with 50, 150, 250, 500, and 1000 ms inter-stimulus intervals

are overlayed. Stimulus artifacts were removed from the traces for clarity. Scale-bars represent 100 ms (horizontal) and 0.3 nA (vertical). (**H**) Paired-pulse ratio (calculated as amplitude of the second response over that of the first response) in wildtype and *Casp3*$^{-/-}$ mice at various inter-stimulus intervals. Mean and standard error of the mean (SEM) are shown. P-values were calculated from Bonferroni's multiple comparison test. p=0.0067 for 50 ms interval, p=0.0369 for 150 ms interval, and p=0.0097 for 250 ms interval. n=16 cells from 7 wildtype mice and n=13 cells from 4 *Casp3*$^{-/-}$ mice.

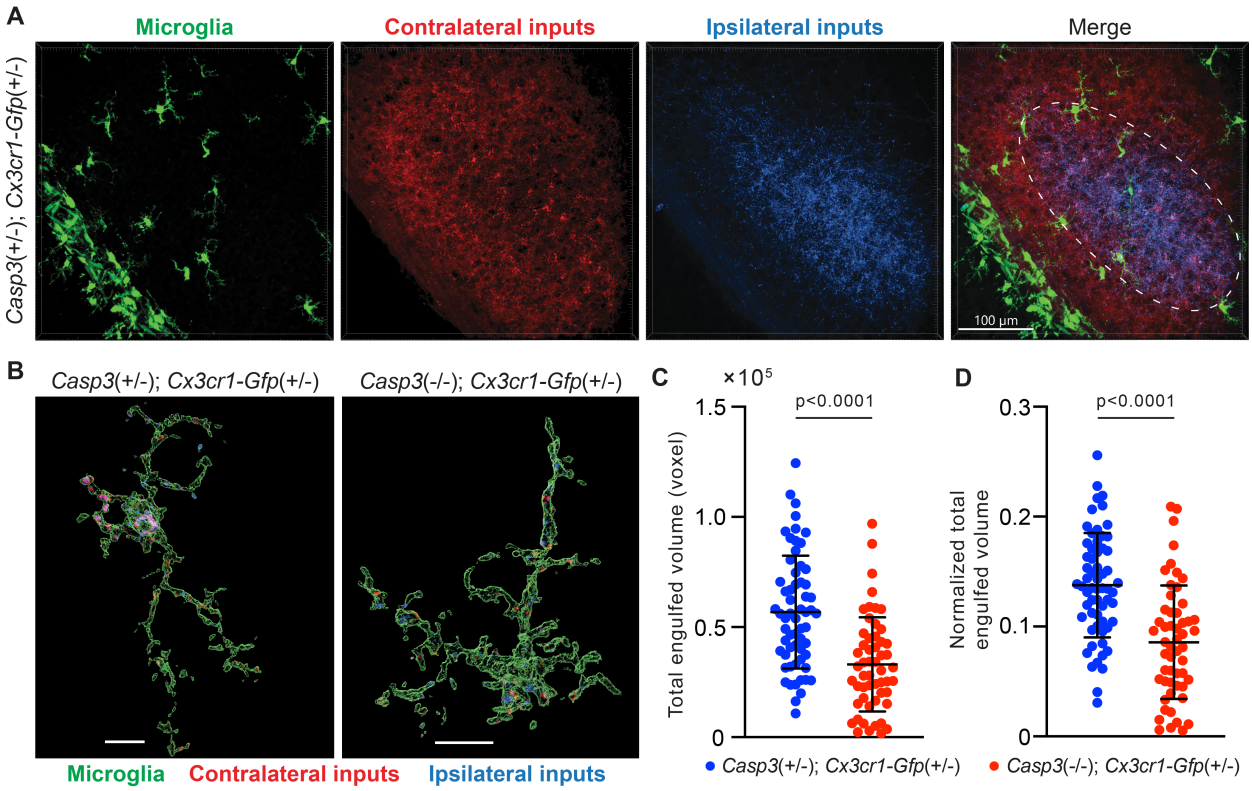

Figure 5. Microglia-mediated synapse elimination depends on caspase-3. (**A**) Representative 3D-reconstructed images of a P5 *Casp3*$^{+/-}$; *Cx3cr1-Gfp*$^{+/-}$ mouse dLGN with microglia displayed in green, contralateral RGC axon terminals in red, and ipsilateral RGC terminals in blue. In the merged image, the region from which microglia are selected for analysis is indicated with the dashed line. The scale-bar represents 100 µm. (**B**) Representative surface rendering of microglia (green) from P5 dLGNs of *Casp3*$^{+/-}$; *Cx3cr1-Gfp*$^{+/-}$ and *Casp3*$^{-/-}$; *Cx3cr1-Gfp*$^{+/-}$ mice. Intracellular contralateral (red) and ipsilateral (blue) RGC axon terminals are shown. Microglia from caspase-3 deficient mice engulf visibly less synaptic material. Scale-bars represent 10 µm. (**C**) Total volume of engulfed synaptic material in individual microglia from *Casp3*$^{+/-}$; *Cx3cr1-Gfp*$^{+/-}$ and *Casp3*$^{-/-}$; *Cx3cr1-Gfp*$^{+/-}$ mice. (**D**) Total volume of engulfed synaptic material in each microglia (from **C**) is normalized to the volume of that microglia. In **C**-**D**, each point represents one microglia. Mean and S.D. are shown. p-values were calculated from unpaired two-tailed t-tests. n=61 microglia from 8 *Casp3*$^{+/-}$; *Cx3cr1-Gfp*$^{+/-}$ mice and n=54 microglia from 5 *Casp3*$^{-/-}$; *Cx3cr1-Gfp*$^{+/-}$ mice.

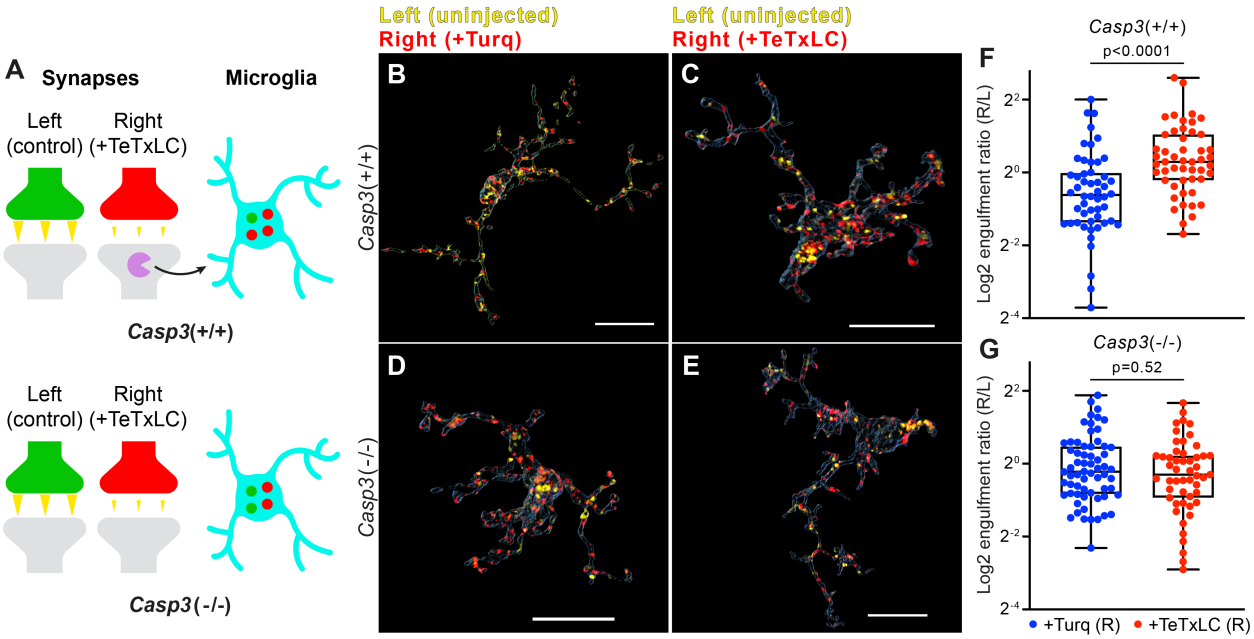

Figure 6. Removal of weak synapses by microglia requires caspase-3 activity. (**A**) Schematics illustrating the experimental rationale. In wildtype mice (upper panel), inactivating retinogeniculate synapses from the right eye activates caspase-3 (magenta) and recruits microglia to preferentially engulf right eye-originated synapses (red) over left eye-originated synapses (green). If caspase-3 activation is blocked (lower panel), engulfment of inactive synapses should be attenuated. (**B-E**) Surface rendering of representative microglia from P5 left dLGN of *Casp3*$^{+/+}$ (**B-C**) or *Casp3*$^{-/-}$ (**D-E**) mice injected with AAV that provided mTurquoise2 (**B** and **D**) or TeTxLC (**C** and **E**) in the right eye at E15. Microglia were labeled by immunostaining against Iba1. RGC axon terminals from the left eye are shown in yellow and terminals from the right eye in red. Scale bars represent 15 μm. (**F-G**) Ratio between volumes of right-eye and left-eye-originated synaptic material engulfed by microglia from *Casp3*$^{+/+}$ (**F**) or *Casp3*$^{-/-}$ (**G**) mice injected with AAV that carried the gene for mTurquoise2 (blue) or TeTxLC (red). Each dot represents one microglia. Engulfment ratios are displayed on a log scale. 0, 25, 50, 75, and 100 percentiles are shown. p-values were calculated from unpaired two-tailed Mann-Whitney tests. n=52 microglia from 7 Turq-injected *Casp3*$^{+/+}$ mice, n=50 microglia from 8 TeTxLC-injected *Casp3*$^{+/+}$ mice, n=64 microglia from 5 Turq-injected *Casp3*$^{-/-}$ mice, and n=51 microglia from 6 TeTxLC-injected *Casp3*$^{-/-}$ mice.

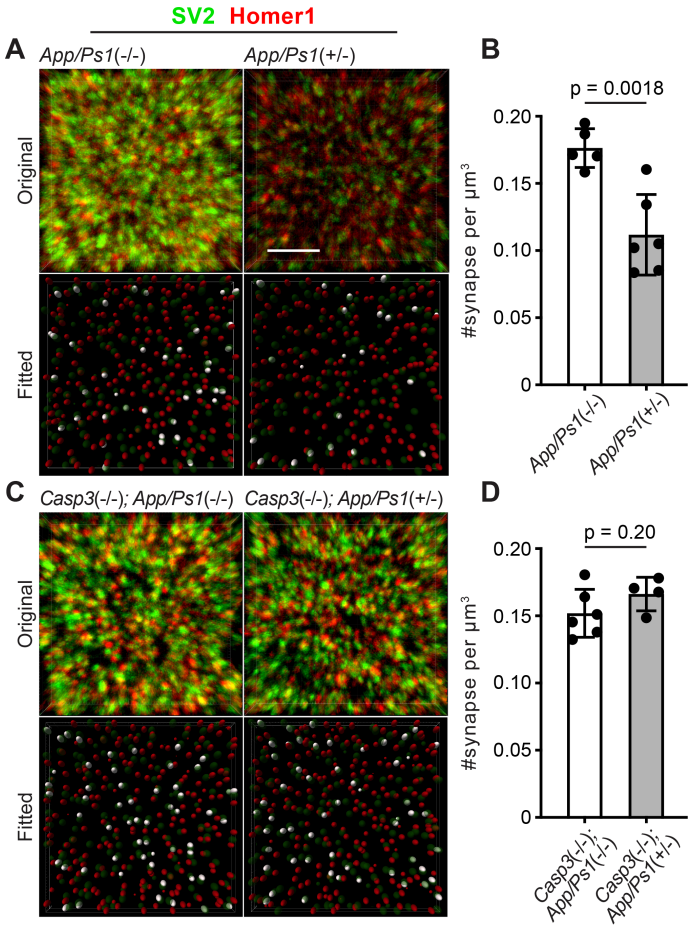

Figure 7. Caspase-3 deficiency protects against Aβ induced synapse loss. (**A** and **C**) Representative 3D-reconstructed images (3 µm in z) showing presynaptic (SV2, in green) and postsynaptic (Homer1, in red) signals in dentate gyrus of female 6 month-old APP/PS1 mice on caspase-3 wildtype (**A**) and deficient (**C**) backgrounds. Ellipsoids were fitted to the original images (upper panels) to isolate pre- (green) and post-synaptic (red) puncta (lower panels). Homer1 ellipsoids found with 300 nm of a SV2 ellipsoid are highlighted in white in the fitted images. Original images are adjusted to the same contrast. For the fitted images, only ellipsoids from the upper half of the z-stack are shown. Scale-bar represents 4 µm. (**B** and **D**) Quantification of synapse density in APP/PS1 mice on caspase-3 wildtype (**B**) and deficient (**D**) backgrounds. Mean and S.D. are shown. p-values were calculated from unpaired two-tailed t-tests. n=5 for *App/Ps1*$^{-/-}$ mice, n=6 for *App/Ps1*$^{+/-}$ mice, n=6 for *Casp3*$^{-/-}$; *App/Ps1*$^{-/-}$ mice, and n=4 for *Casp3*$^{-/-}$; *App/Ps1*$^{+/-}$ mice.